This paper is published as part of a PCCP Themed Issue on:

Modern EPR Spectroscopy: Beyond the EPR Spectrum

Guest Editor: Daniella Goldfarb

Editorial

Perspective

Communication

Papers

A W-band pulsed EPR/ENDOR study of $Co^{II}S_4$ coordination in the $Co[(SPPh_2)(SP^iPr_2)N]_2$ complex
Silvia Sottini, Guinevere Mathies, Peter Gast, Dimitrios Maganas, Panayotis Kyritsis and Edgar J.J. Groenen, *Phys. Chem. Chem. Phys.*, 2009
DOI: 10.1039/b905726a

Exchangeable oxygens in the vicinity of the molybdenum center of the high-pH form of sulfite oxidase and sulfite dehydrogenase
Andrei V. Astashkin, Eric L. Klein, Dmitry Ganyushin, Kayunta Johnson-Winters, Frank Neese, Ulrike Kappler and John H. Enemark, *Phys. Chem. Chem. Phys.*, 2009
DOI: 10.1039/b907029j

Magnetic quantum tunneling: key insights from multi-dimensional high-field EPR
J. Lawrence, E.-C. Yang, D. N. Hendrickson and S. Hill, *Phys. Chem. Chem. Phys.*, 2009
DOI: 10.1039/b908460f

Spin-dynamics of the spin-correlated radical pair in photosystem I. Pulsed time-resolved EPR at high magnetic field
O. G. Poluektov, S. V. Paschenko and L. M. Utschig, *Phys. Chem. Chem. Phys.*, 2009
DOI: 10.1039/b906521k

Enantioselective binding of structural epoxide isomers by a chiral vanadyl salen complex: a pulsed EPR, cw-ENDOR and DFT investigation
Damien M. Murphy, Ian A. Fallis, Emma Carter, David J. Willock, James Landon, Sabine Van Doorslaer and Evi Vinck, *Phys. Chem. Chem. Phys.*, 2009
DOI: 10.1039/b907807j

Topology of the amphipathic helices of the colicin A pore-forming domain in *E. coli* lipid membranes studied by pulse EPR
Sabine Böhme, Pulagam V. L. Padmavathi, Julia Holterhues, Fatiha Ouchni, Johann P. Klare and Heinz-Jürgen Steinhoff, *Phys. Chem. Chem. Phys.*, 2009
DOI: 10.1039/b907117m

Structural characterization of a highly active superoxide-dismutase mimic
Vimalkumar Balasubramanian, Maria Ezhevskaya, Hans Moons, Markus Neuburger, Carol Cristescu, Sabine Van Doorslaer and Cornelia Palivan, *Phys. Chem. Chem. Phys.*, 2009
DOI: 10.1039/b905593b

Structure of the oxygen-evolving complex of photosystem II: information on the S_2 state through quantum chemical calculation of its magnetic properties
Dimitrios A. Pantazis, Maylis Orio, Taras Petrenko, Samir Zein, Wolfgang Lubitz, Johannes Messinger and Frank Neese, *Phys. Chem. Chem. Phys.*, 2009
DOI: 10.1039/b907038a

Population transfer for signal enhancement in pulsed EPR experiments on half integer high spin systems
Ilia Kaminker, Alexey Potapov, Akiva Feintuch, Shimon Vega and Daniella Goldfarb, *Phys. Chem. Chem. Phys.*, 2009
DOI: 10.1039/b906177k

The reduced [2Fe-2S] clusters in adrenodoxin and *Arthrospira platensis* ferredoxin share spin density with protein nitrogens, probed using 2D ESEEM
Sergei A. Dikanov, Rimma I. Samoilova, Reinhard Kappl, Antony R. Crofts and Jürgen Hüttermann, *Phys. Chem. Chem. Phys.*, 2009
DOI: 10.1039/b904597j

Frequency domain Fourier transform THz-EPR on single molecule magnets using coherent synchrotron radiation
Alexander Schnegg, Jan Behrends, Klaus Lips, Robert Bittl and Karsten Holldack, *Phys. Chem. Chem. Phys.*, 2009
DOI: 10.1039/b905745e

PELDOR study of conformations of double-spin-labeled single- and double-stranded DNA with non-nucleotide inserts
Nikita A. Kuznetsov, Alexandr D. Milov, Vladimir V. Koval, Rimma I. Samoilova, Yuri A. Grishin, Dmitry G. Knorre, Yuri D. Tsvetkov, Olga S. Fedorova and Sergei A. Dzuba, *Phys. Chem. Chem. Phys.*, 2009
DOI: 10.1039/b904873a

Site-specific dynamic nuclear polarization of hydration water as a generally applicable approach to monitor protein aggregation
Anna Pavlova, Evan R. McCarney, Dylan W. Peterson, Frederick W. Dahlquist, John Lew and Songi Han, *Phys. Chem. Chem. Phys.*, 2009
DOI: 10.1039/b906101k

Structural information from orientationally selective DEER spectroscopy
J. E. Lovett, A. M. Bowen, C. R. Timmel, M. W. Jones, J. R. Dilworth, D. Caprotti, S. G. Bell, L. L. Wong and J. Harmer, *Phys. Chem. Chem. Phys.*, 2009
DOI: 10.1039/b907010a

Structure and bonding of $[V^{IV}O(acac)_2]$ on the surface of AlF_3 as studied by pulsed electron nuclear double resonance and hyperfine sublevel correlation spectroscopy
Vijayasarathi Nagarajan, Barbara Müller, Oksana Storcheva, Klaus Köhler and Andreas Pöppl, *Phys. Chem. Chem. Phys.*, 2009
DOI: 10.1039/b903826b

Local variations in defect polarization and covalent bonding in ferroelectric Cu2+-doped PZT and KNN functional ceramics at themorphotropic phase boundary
Rüdiger-A. Eichel, Ebru Erünal, Michael D. Drahus, Donald M. Smyth, Johan van Tol, Jérôme Acker, Hans Kungl and Michael J. Hoffmann, *Phys. Chem. Chem. Phys.*, 2009
DOI: 10.1039/b905642d

Dynamic nuclear polarization coupling factors calculated from molecular dynamics simulations of a nitroxide radical in water

Deniz Sezer, M. J. Prandolini and Thomas F. Prisner*

Received 20th March 2009, Accepted 15th June 2009
First published as an Advance Article on the web 6th July 2009
DOI: 10.1039/b905709a

The magnetic resonance signal obtained from nuclear spins is strongly affected by the presence of nearby electronic spins. This effect finds application in biomedical imaging and structural characterization of large biomolecules. In many of these applications nitroxide free radicals are widely used due to their non-toxicity and versatility as site-specific spin labels. We perform molecular dynamics simulations to study the electron–nucleus interaction of the nitroxide radical TEMPOL and water in atomistic detail. Correlation functions corresponding to the dipolar and scalar spin–spin couplings are computed from the simulations. The dynamic nuclear polarization coupling factors deduced from these correlation functions are in good agreement with experiment over a broad range of magnetic field strengths. The present approach can be applied to study solute–solvent interactions in general, and to characterize solvent dynamics on the surfaces of proteins or other spin-labeled biomolecules in particular.

I. Introduction

Nuclear and electronic spins couple to applied magnetic fields with coupling strengths determined by the respective magnetogyric ratios γ_n and γ_e. Typically, the interaction of the magnetic field with the electronic spins is orders of magnitude stronger than its coupling to nuclear spins. In the case of a free electron and a proton, for example, $\gamma_e/\gamma_n \approx -660$. This difference is advantageously exploited in dynamic nuclear polarization (DNP) experiments of liquid solutions containing paramagnetic centers. In such experiments the electron spin magnetization is brought out of equilibrium by continuously irradiating the sample with microwaves at the appropriate frequency. The resulting steady-state electronic magnetization polarizes the nuclear spins under the action of the existing electron–nucleus (dipolar and/or exchange) spin interactions. In this way nuclear magnetizations up to γ_e/γ_n times larger than their values at thermal equilibrium can be obtained.

Traditionally DNP enhancement measurements have been used to study the dynamics of solute–solvent interactions.[1–3] Experiments with small organic radicals in liquid solutions have been performed and the results have been rationalized in terms of translational and rotational relative motion of the spin-bearing species.[1,2]

Recently DNP has attracted renewed attention as means to significantly enhance the sensitivity in the imaging of small organic molecules for the purposes of biomedical applications using nuclear magnetic resonance (NMR).[4] In addition, its applicability to the structural and functional characterization of biomolecules by NMR spectroscopy is currently being investigated and developed.[5,6] The high magnetic fields employed in biomolecular NMR studies render the technological aspect of the corresponding DNP experiments particularly challenging.[7] Leaving the difficulties related to the hardware aside, a major argument against the development of high-field DNP has been the understanding that the enhancement drops to essentially zero at the magnetic fields of interest for high-resolution NMR. Strong support for this view comes from the picture of relative solvent–solute motion offered by the aforementioned models of translational and rotational diffusion.

It is only in the last year that DNP enhancements have been actually measured for small nitroxides in aqueous solution at 3.4 and 9.2 T.[5,6,8] The results indicate that although the enhancements do decrease substantially at these higher magnetic fields, they are large enough to be of significant practical interest. Rationalizing the origin of the observed reasonably large high-field DNP enhancements calls for a treatment of the relative molecular motion on time scales as short as a fraction of a picosecond. Probing molecular dynamics on sub-picosecond time scales, high-field DNP experiments are extremely sensitive to the atomistic details of the polarizing agent and the solvent and of their relative motion. Such details are clearly not present in the analytical models used to interpret the data, in which it is assumed that the spins are localized at the center of spherical spin-bearing molecules which undergo relative translational and rotational motions characterized by a single diffusion coefficient.

Molecular dynamics (MD) simulations appear to be perfectly suited to address these difficulties since they allow for the atomically-detailed description of the solute–solvent dynamics on sub-picosecond time scales. Spin relaxation due to *nuclear* dipole–dipole coupling has been studied with MD for liquid acetonitrile,[9] xenon in benzene,[10] or a Lennard-Jones fluid.[11] Such studies offer a detailed picture of the translational and rotational contribution to the relaxation and provide an opportunity to compare with the predictions of analytical models or directly with experiments. However, bearing in mind that the nuclear Larmor time scale is on the

Institut für Physikalische und Theoretische Chemie, J. W. Goethe-Universität, 60438 Frankfurt am Main, Germany. E-mail: prisner@chemie.uni-frankfurt.de

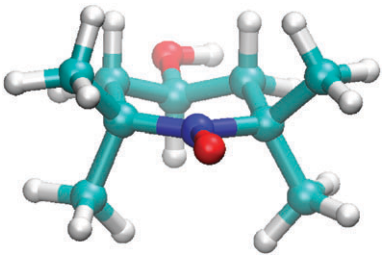

Fig. 1 The nitroxide radical TEMPOL.

order of nanoseconds, it becomes evident that what is really tested for these systems, in which the relative motion is rather fast, is the integrated area under the dipole–dipole correlation function. In contrast, the electronic Larmor precession is on the order of a few picoseconds or less. Therefore, as already alluded to, the electron–nucleus dipole–dipole correlation function probes not only the slow solute–solvent dynamics but also its faster details. From that perspective, the comparison between calculated DNP coupling factors and experiment is an extremely stringent test on the ability of MD simulations to properly capture the amplitude of the solute–solvent dynamics over a wide range of time scales.

In this paper we perform molecular dynamics simulations to calculate the DNP coupling factor between the unpaired electron on a nitroxide radical and the protons of water. We study the nitroxide radical TEMPOL (4-hydroxy-2,2,6,6-tetramethylpiperidine-1-oxyl, Fig. 1), which has been used recently in DNP enhancement experiments at high fields.[5,6,8] The present paper is a part of our more extensive effort to provide rigorous description of the various aspects of high-field DNP. These include the realistic treatment of the solute–solvent dynamics responsible for the magnitude of the coupling factor, proper treatment of the relaxation mechanisms which determine to what extent the electron spin magnetization can be brought out of equilibrium (subject of the companion paper II; DOI: 10.1039/b906719c), and assessing the possibility of achieving even larger DNP enhancements using biradicals.

The paper is organized as follows. The necessary theoretical background is reviewed in section II. Section III contains information about the computational methods employed. The presentation of our results, given in section IV, is followed by discussion (section V) and conclusion (section VI).

II. Theoretical background

A DNP enhancement

In the dynamic polarization of water protons by nitroxide free radicals one aims to increase the steady-state nuclear magnetization using the dipolar and/or scalar interactions between the nuclear and electronic spins. The electron–nucleus dipolar and scalar couplings can be summarized by the interaction Hamiltonian[1,2] (in units of angular frequency)

$$\hat{H}_{SI}(t) = \hat{\boldsymbol{S}}\cdot D(t)\cdot\hat{\boldsymbol{I}} + A(t)\hat{\boldsymbol{S}}\cdot\hat{\boldsymbol{I}} \qquad (1)$$

where $\hat{\boldsymbol{S}}$ and $\hat{\boldsymbol{I}}$ denote the electronic and nuclear spin operators, and $D(t)$ and $A(t)$ are the instantaneous values of the dipolar coupling tensor and the scalar coupling, respectively. When the two spins are sufficiently far apart and can be treated as point dipoles, the dipolar coupling tensor is expressed as

$$D(t) = \delta\frac{E - 3\underline{\boldsymbol{r}}(t)\underline{\boldsymbol{r}}(t)}{r^3(t)}, \qquad (2)$$

where E is the 3×3 identity matrix, $r(t)$ is the magnitude and $\underline{\boldsymbol{r}}(t)$ the direction of the vector $\boldsymbol{r}(t)$, pointing from one of the spins to the other. The prefactor is

$$\delta = (\mu_0/4\pi)\hbar\gamma_S\gamma_I, \qquad (3)$$

where μ_0 is the magnetic permeability of free space, $\hbar$ is Planck's constant divided by 2π, and γ_S and γ_I are the electron and nuclear magnetogyric ratios. The scalar coupling, on the other hand, depends on the probability density of the unpaired electron at the nucleus. It is therefore expected to be of significant strength only when the solvent is in close contact with the radical, as in the case of hydrogen bonding between the nitroxide and water.

When the interaction of the nuclear spin with the spin of the unpaired electron is described by the Hamiltonian (1), the longitudinal nuclear magnetization $\langle\hat{I}_z\rangle$ is found to obey the Solomon equation[12]

$$\frac{\mathrm{d}}{\mathrm{d}t}\langle\hat{I}_z\rangle = -R_1^{II}(\langle\hat{I}_z\rangle - I_0) - R_1^{IS}(\langle\hat{S}_z\rangle - S_0), \qquad (4)$$

where $I_0 = \langle\hat{I}_z\rangle_0$ and $S_0 = \langle\hat{S}_z\rangle_0$ denote the equilibrium values of the nuclear and electronic magnetizations, and R_1^{II} and R_1^{IS} are certain relaxation rates, to be specified below. An additional relaxation rate, R_1^0, needs to be included in eqn (4) to account for processes that lead to the relaxation of the nuclear magnetization but are not related to the presence of the electronic spins. This is achieved by replacing R_1^{II} in eqn (4) with

$$R_1 = R_1^{II} + R_1^0. \qquad (5)$$

The degree by which the nuclear magnetization under steady-state DNP conditions, $I_{ss} = \langle\hat{I}_z\rangle_{ss}$, is larger than the equilibrium magnetization in the absence of the polarizing paramagnetic species, I_0, is characterized by the DNP enhancement[1]

$$\varepsilon = (I_{ss} - I_0)/I_0. \qquad (6)$$

It can be calculated from the steady-state solution of eqn (4). The latter is readily put in the form[1]

$$I_{ss} = I_0\left(1 + \frac{R_1^{IS}}{R_1^{II}}\frac{S_0 - S_{ss}}{S_0}\frac{R_1^{II}}{R_1}\frac{S_0}{I_0}\right), \qquad (7)$$

with $S_{ss} = \langle\hat{S}_z\rangle_{ss}$. It is convenient to define the coupling, the saturation and the leakage factors, respectively, as

$$\begin{aligned}\xi &= R_1^{IS}/R_1^{II}\\ s &= (S_0 - S_{ss})/S_0,\\ f &= R_1^{II}/R_1 = 1 - R_1^0/R_1.\end{aligned} \qquad (8)$$

After replacing the ratio of the equilibrium electronic and nuclear magnetizations, S_0/I_0, by γ_S/γ_I and using the definition of ε, eqn (7) leads to

$$\varepsilon = \xi sf\gamma_S/\gamma_I. \qquad (9)$$

Since ξ, s and f are all smaller than or equal to one, the maximum achievable DNP enhancement is γ_S/γ_I, as was already mentioned in the introduction.

B Coupling factor and correlation functions

The dependence of the coupling factor on the relative solvent–nitroxide dynamics is through the spectral densities $J^{(m)}(\omega)$ and $K(\omega)$ corresponding to, respectively, dipolar and scalar electron–nucleus interactions. The former are defined as the real part of the (one-sided) Fourier transform,

$$J^{(m)}(\omega) = \mathrm{Re}\int_0^\infty \mathrm{d}\tau C^{(m)}(\tau)\mathrm{e}^{-\mathrm{i}\omega\tau}, \qquad (10)$$

of the time correlation functions

$$C^{(m)}(\tau) = \overline{F^{(m)}(\boldsymbol{r}(t))F^{(m)*}(\boldsymbol{r}(t+\tau))}. \qquad (11)$$

Here

$$F^{(0)}(\boldsymbol{r}) = \sqrt{\frac{3}{2}}\frac{(r^2-3r_z^2)}{r^5},\ F^{(1)}(\boldsymbol{r}) = 3\frac{r_z(r_x+\mathrm{i}r_y)}{r^5},$$
$$F^{(2)}(\boldsymbol{r}) = -\frac{3}{2}\frac{(r_x-\mathrm{i}r_y)^2}{r^5} \qquad (12)$$

are the rank-2 spherical components of the dipolar tensor (2) divided by δ, and r_x, r_y, r_z are the Cartesian components of $\boldsymbol{r}$. The line above the Fs in eqn (11) denotes a double average over time and all the protons in the system. Similarly, the spectral density corresponding to the scalar coupling is

$$K(\omega) = \mathrm{Re}\int_0^\infty \mathrm{d}\tau\overline{A(t-\tau)A(t)}\mathrm{e}^{-\mathrm{i}\omega\tau}. \qquad (13)$$

Unlike the dipolar functions $F^{(m)}$, the scalar coupling A is hard to express formally. A functional form which is commonly used to model the rapid decrease of A with the separation between the two spins is[13]

$$A(t) = A_0\mathrm{e}^{-\lambda(r(t)-r_0)}, \qquad (14)$$

where A_0, r_0 and λ are free parameters that need to be chosen appropriately.

The spectral densities enter into the coupling factor through the relaxation rates R_1^{II} and R_1^{IS}, which for an electronic spin $S = 1/2$ and a proton nuclear spin $I = 1/2$ are found to be[1,2,12]

$$R_1^{II} = \frac{\delta^2}{12}[J^{(0)}(\omega_I-\omega_S) + 3J^{(1)}(\omega_I) + 6J^{(2)}(\omega_I+\omega_S)] + K(\omega_I-\omega_S)/2,$$
$$R_1^{IS} = \frac{\delta^2}{12}[6J^{(2)}(\omega_I+\omega_S) - J^{(0)}(\omega_I-\omega_S)] - K(\omega_I-\omega_S)/2. \qquad (15)$$

In these expressions, the spectral densities are evaluated at the specified combinations of the electronic and nuclear Larmor (angular) frequencies ω_S and ω_I. The arguments of $J^{(0)}$, $J^{(2)}$, and K imply simultaneous flips of the electron and proton spins (zero and double quantum coherence), whereas the argument of $J^{(1)}$ implies a flip of the proton spin only (single quantum coherence). The frequencies $f = \omega/2\pi$ are listed in Table 1 for several values of the magnetic field in a range of experimental interest.

Table 1 Electronic (S) and nuclear (^{1}H, I) Larmor frequencies, $f = \omega/2\pi$ and associated time scales, $\tau = 1/\omega$, for various magnetic field strengths

B/Tesla	0.342	1.21	3.35	6.4	9.2	12.8
f_S/GHz	9.6	34	94	180	260	360
τ_S/ps	17	4.7	1.7	0.88	0.61	0.44
f_I/MHz	15	50	140	270	390	540
τ_I/ns	11	3.1	1.1	0.58	0.40	0.29

The contribution of the scalar coupling in (15) assumes scalar relaxation of the first kind, according to the nomenclature of ref. 12 (*i.e.*, the parameter β of ref. 1 is equal to zero). For this to be the case, the time scale on which the scalar coupling is modulated has to be much shorter than the T_1 and T_2 relaxation times of the electron. As will become apparent in section IV, the former time scale is in the picosecond range, whereas electronic T_1 and T_2 are on the order of hundreds and tens of nanoseconds, respectively.

Taking into account the fact that the spectral densities are even functions of their argument, and $\omega_S \gg \omega_I$, the DNP coupling parameter can be approximated by

$$\xi \approx \frac{6J^{(2)}(\omega_S) - J^{(0)}(\omega_S) - 6K(\omega_S)/\delta^2}{J^{(0)}(\omega_S) + 3J^{(1)}(\omega_I) + 6J^{(2)}(\omega_S) + 6K(\omega_S)/\delta^2}. \qquad (16)$$

Substantial experimental evidence exists for nitroxides in water indicating that the observed proton DNP enhancement can be rationalized entirely in terms of dipolar electron–nucleus coupling, disregarding the scalar coupling completely.[2] Our estimates, presented in section IV, confirm that the last term in the numerator and the denominator of (16) is negligible compared to the others.

In isotropic environments the three dipolar spectral densities $J^{(m)}$ are all equal. Therefore, one can drop the superscript m and work with a single spectral density J. The coupling factor then becomes

$$\xi \approx \frac{5J(\omega_S)}{3J(\omega_I) + 7J(\omega_S)}, \qquad (17)$$

where the approximation consists of neglecting the effect of the scalar coupling in eqn (16). The maximum achievable coupling factor of 1/2 for dipolar coupled spins follows from eqn (17) under the assumption that the Larmor precession time scale of the electron is much longer than the time scales of the classical motion, thus yielding $J(\omega_S) \approx J(\omega_I) \approx J(0)$. This condition is expected to be no longer satisfied at frequencies about and higher than 9 GHz for which the Larmor time scales drop to a few picoseconds and less (Table 1). In comparison, the Larmor precession of the proton nuclear spin is about three orders of magnitude slower, which may justify the approximation

$$J(\omega_I) \approx J(0) = \mathrm{const}. \qquad (18)$$

Whereas the numerator in eqn (17) contains only spectral densities at the electron Larmor frequency the denominator contains a spectral density evaluated at the low nuclear Larmor frequency ω_I. Therefore, for the calculation of ξ one needs not only the initial decay of the correlation functions but

also their long-time tail. The implication for the MD simulations is that the motion of the water protons relative to the nitroxide has to be followed for long enough times and up to sufficiently large distances. In other words, the simulated system has to be large enough and contain sufficiently many solvent molecules, as is well appreciated in the literature.[11] Because the nuclear Larmor time scale drops to a few hundreds of picoseconds at the higher fields that we consider (Table 1), we retain the argument ω_I when calculating the coupling factor using eqn (17).

C Estimating coupling factors from NMRD data

Until recently,[14,15] the method of choice for accessing DNP coupling factors experimentally has been nuclear magnetic relaxation dispersion (NMRD) measurements. The approach, discussed in ref. 1 for purely dipolar interaction between the electron and nuclear spins, has been utilized recently to determine the coupling factors of TEMPOL in water at 9.6, 94 GHz,[5] and 260 GHz.[8] It is based on the observation that the denominator of the coupling factor, R_1^{II}, already contains in itself the value of the numerator, R_1^{IS}. At any magnetic field strength, R_1^{II} can be determined experimentally by measuring the T_1 of the water protons with and without the radical and subtracting the latter from the former [*cf.* eqn (5)]. To obtain R_1^{IS} from the determined R_1^{II} it is necessary to subtract the part of R_1^{II} that corresponds to $3J(\omega_I)$ in the denominator of eqn (17). Using the approximation (18) and denoting the (constant) contribution of $3J(0)$ to R_1^{II} by $2\omega_1$, eqn (17) can be put into the form[1,5]

$$\xi_{\mathrm{NMRD}} \approx \frac{5}{7}\frac{R_1^{II} - 2w_1}{R_1^{II}} = \frac{5}{7}\left(1 - \frac{2\omega_1}{R_1 - R_1^0}\right). \qquad (19)$$

The constant $2\omega_1$ can be estimated from T_1 measurements at very low magnetic fields,[1] however, these details are not relevant for the purposes of the present discussion.

Instead of eqn (19), which is written in terms of experimentally accessible quantities, the following equivalent expression is more appropriate in our case:

$$\xi_{\mathrm{NMRD}} \approx \frac{5}{7}\frac{3J(\omega_I) + 7J(\omega_S) - X}{3J(\omega_I) + 7J(\omega_S)}. \qquad (20)$$

Here, the relaxation rates have been replaced by the computationally accessible spectral densities, and the constant $2\omega_1$ (rescaled appropriately) has been denoted by X. It is evident that the latter expression reduces to the correct coupling factor, eqn (17), when $X = 3J(\omega_I)$. However, $J(\omega_I)$ at the frequency of interest is typically not known. As mentioned above, it was taken as a constant in ref. 5 to estimate the coupling factors from NMRD. The same constant was utilized in ref. 8.

We would like to point out that beyond the mentioned approximations no motional model needs to be assumed for this analysis. If desired, a model can be employed to follow the frequency dependence of $2\omega_1$ (or X) which, formally, should not be a constant. These observations will be important when we compare the coupling factors calculated from MD with the corresponding NMRD estimates in section IVD.

D Analytical force-free model of translational diffusion

A dynamical model which is commonly invoked to rationalize the relation between the DNP coupling factors and the underlying molecular motions is the analytical force-free (FF) model.[16–18] This model was used in the interpretation of DNP data with trityl[4] and nitroxide[5] radicals. The model assumes that the interacting spins are situated at the centers of spherical spin-bearing molecules which undergo translational diffusion with respect to each other. Denoting the translational diffusion coefficient by D_{ff} and the distance of closest approach of the spins by d_{ff} the characteristic correlation time scale of the FF model is

$$\tau_{\mathrm{ff}} = d_{\mathrm{ff}}^2/D_{\mathrm{ff}}. \qquad (21)$$

In terms of τ_{ff} the spectral density of the model is[18–21]

$$J_{\mathrm{ff}}(\omega) \propto \frac{\sum_{n=0}^{2} c_n (2\omega\tau_{\mathrm{ff}})^{\frac{n}{2}}}{\sum_{n=0}^{6} d_n (2\omega\tau_{\mathrm{ff}})^{\frac{n}{2}}}, \qquad (22)$$

with $c_0 = 8$, $c_1 = 5$, $c_2 = 1$, and $d_0 = 81$, $d_1 = 81$, $d_2 = 81/2$, $d_3 = 27/2$, $d_4 = 4$, $d_5 = 1$, and $d_6 = 1/8$. [The proportionality constant is not important for calculating the coupling factor according to eqn (17).]

The explicit form of the analytical correlation function that leads to the spectral densities (22) is not of interest to us. However, we note that at long times it does not decay exponentially but goes like $\sim\tau^{-3/2}$.[11] In spite of its simplifying assumptions, the FF model of translational diffusion is expected to be rather accurate for long times, when the water molecules have diffused far away from their starting positions. Therefore, the correlation functions extracted from MD should also satisfy the asymptotic power-law behavior. Given the finite size of the simulated system and the finite simulation time, however, we expect that the long-time tails of the MD correlation functions will be too noisy to properly reflect the expected asymptotic behaviour. For the calculation of the coupling factors, therefore, we explicitly impose the $\sim\tau^{-3/2}$ condition on the correlation functions.

III. Methods

A MD simulation details and calibration of the water diffusion

The simulated system was a cubic box filled with TIP3P[22] waters and one TEMPOL molecule. The simulations were performed with the MD simulation package NAMD,[23] under constant temperature and volume (NVT ensemble), using periodic boundary conditions. The electrostatic interactions were treated with particle mesh Ewald.[24,25] Bonds involving hydrogen atoms were constrained with SETTLE[26] and a 2 fs time step was used for the numerical integration. The simulations lasted for 2.1 ns. Coordinates were saved every 75 integration steps (0.15 ps) for subsequent analysis. The first 600 snapshots (90 ps) were excluded from the analysis. Simulations were carried out at three different temperatures, $T = 298$ K (25 °C), 308 K (35 °C), and 318 K (45 °C), and with $N = 1000$ or 3000 water molecules. The target water densities at these temperatures, *i.e.*, 0.997 g cm^{-3} (25 °C), 0.994 g cm^{-3} (35 °C), and 0.990 g cm^{-3} (45 °C), were achieved by fixing the

Table 2 Box sizes L (Å) for the systems simulated at temperature T (°C) and containing N TIP3P waters

N	1000			3000		
T	25	35	45	25	35	45
L	31.076	31.107	31.148	44.819	44.865	44.923

size of the cubic box to the values given in Table 2. The temperature was controlled with a Langevin thermostat, which was coupled only to the heavy atoms.

It is well known that the TIP3P water model (like any other nonpolarizable water model) leads to faster water dynamics.[27] In particular, the translational self-diffusion coefficient of the TIP3P water model at 25 °C is about 5.7×10^{-9},[28] whereas the experimental value is 2.3×10^{-9} m^2 s^{-1}.[29] Because the DNP coupling factor is expected to be strongly sensitive to the relative translational diffusion of the radical and water,[16] this deficiency of the water model was unacceptable for our purposes. In an effort to overcome the problem within the constraints of the available nonpolarizable force field, we adjusted the friction coefficient of the thermostat such that the translational dynamics of the TIP3P waters was sufficiently slowed down for their diffusion coefficient to match the experimental value. The calibration of the friction coefficient was performed on the smaller systems with $N = 1000$ waters.

The translational diffusion coefficient of water was calculated from the mean square displacement of the water oxygens using the relation

$$\lim_{\tau\to\infty} \overline{|\boldsymbol{r}(t+\tau) - \boldsymbol{r}(t)|^2} = 6D_{\mathrm{w}}\tau, \qquad (23)$$

where $\boldsymbol{r}(t)$ is the oxygen position at time t (after "undoing" the effect of the periodic boundary conditions), and the average is over all the waters present in the simulation and over all times t. The finite duration of the simulated trajectories implies that for larger values of τ there are less initial times t to sum over. Therefore, the uncertainty in the estimate of D_{w} increases with τ. On the other hand, τ should be long enough for the water translation to be purely diffusive. To have a feeling of the uncertainties, we used the fact that the diffusion coefficients along three arbitrary but orthogonal directions x, y and z are all expected to be equal. Therefore, at sufficiently long τ, the three ratios

$$D_i(\tau) = \overline{|r_i(t+\tau) - r_i(t)|^2}/2\tau, \; i = x, y, z, \qquad (24)$$

should provide three independent estimates of D_{w}.

In Fig. 2 we plot the average of D_x, D_y and D_z, as well as their standard deviation about this average calculated from the simulations. It is seen that the experimental values of the diffusion coefficient are attained with Langevin friction $\gamma = 11$ ps^{-1} at 25 °C, $\gamma = 9$ ps^{-1} at 35 °C, and $\gamma = 7.5$ ps^{-1} at 45 °C. The plot also allows us to estimate the uncertainty of the calculated D_{w}.

For the calculation of the DNP coupling factor one TEMPOL molecule was inserted at the center of the larger water boxes with $N = 3000$ molecules. This was done by removing the water molecules with oxygen atoms closer than 2.0 Å to the TEMPOL heavy atoms. Nine such waters were removed, leading to 2991 waters in the final systems. The

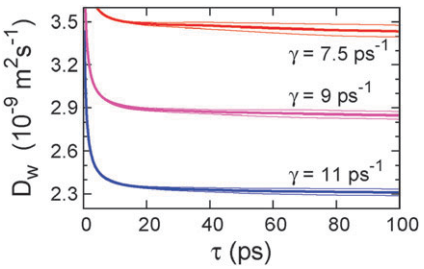

Fig. 2 Calculated self-diffusion coefficients for water at $T = 25$ °C ($\gamma = 11$ ps^{-1}), 35 °C ($\gamma = 9$ ps^{-1}) and 45 °C ($\gamma = 7.5$ ps^{-1}). The targeted experimental values are respectively 2.3×10^{-9}, 2.9×10^{-9} and 3.5×10^{-9} m^2 s^{-1}.[29] The thin lines correspond to one standard deviation about the average, indicated with a thick line.

friction coefficients used in the simulations at the three temperatures were set to the values determined previously using the water boxes with 1000 waters.

The parametrization of the nitroxide radical TEMPO had been reported previously.[30] A standard OH group from the CHARMM force field[31,32] was appended to TEMPO to obtain the parameters of TEMPOL used in the current study.

B *Ab initio* computations and calculation of the correlation functions

In order to assess the magnitude of the scalar electron–nucleus coupling several nitroxide–water interaction geometries, shown in Fig. 3, were analyzed by performing *ab initio* calculations. All the calculations were carried with the program *Gaussian 03*[33] for the closely related nitroxide TEMPO (2,2,6,6-tetramethylpiperidine-1-oxyl), as was previously reported in ref. 30. The relative orientation of the water molecule with respect to the nitroxide was optimized keeping the structure of TEMPO and the structure of the water molecule fixed, the former at the B3LYP/6-31G* optimized geometry and the latter at the experimental geometry.[34] The optimization was performed using B3LYP/6-311++G**, a level of theory which, reportedly, is sufficient to accurately reproduce hydrogen bond geometries.[35] A subsequent single-point energy evaluation was performed using B3LYP/aug-cc-pvdz. For further details the reader is referred to ref. 30.

Conformations in which the water hydrogen is positioned close to the p_z orbital occupied by the unpaired electron (positions 2 and 4 in Fig. 3) are expected to result in larger electron density at the proton nucleus compared to conformations in which the hydrogen lies in the plane approximately perpendicular to the p_z orbital (positions 1 and 3). The

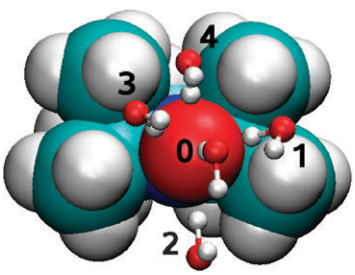

Fig. 3 Optimal TEMPO–water interaction geometries.[30]

water–nitroxide interaction energies for conformations 1 to 4 were found to be similar and about 1 kcal mol^{-1} higher than for the geometry in which one of the water hydrogens is along the N–O bond of the nitroxide moiety (position 0).[30] The scalar couplings according to the *ab initio* calculations are given in Table 3 for the two different basis sets. As expected, the couplings are largest for the dimer geometries 2 and 4. Five to ten times smaller couplings were computed for the other three conformations. The differences between the scalar couplings in columns bs1 and bs2 of Table 3 reflect the degree of basis set dependence.

The dependence of the computed scalar couplings on the geometry of the hydrogen-bonded water–nitroxide system that emerges from the data in Table 3 is clearly beyond the reach of a model which takes into consideration only the hydrogen bond distance, such as the one in eqn (14). (The proton–oxygen distances for the conformations from 0 to 4 were respectively 1.97, 1.90, 1.94, 1.91, and 1.91 Å.[30]) However, it would be hard to properly account for this dependence in the framework of classical MD simulations. Therefore, hoping to obtain an order-of-magnitude estimate of the relative importance of the scalar coupling with respect to the dipolar coupling, we decided to employ the functional form of eqn (14). On the basis of the values in Table 3, we concluded that $A_0 = 3$ MHz and $r_0 = 1.9$ Å should constitute a reasonable choice. To be on the safe side with our estimate, the strength of the scalar coupling was chosen to reflect the larger values in Table 3. We further selected $\lambda^{-1} = 0.8$ Å as a reasonable distance over which the magnitude of the scalar coupling drops.

The dipolar electron–proton couplings according to the *ab initio* calculations are also shown in Table 3. The numerical values are pretty much identical for the two different basis sets. Again, thinking about the p_z orbital occupied by the unpaired electron, it is possible to rationalize the larger dipolar coupling for conformations 2 and 4.

An issue that becomes immediately apparent when one wants to calculate the dipolar correlation functions $C^{(m)}(\tau)$ from MD simulations is the choice of the electron spin position on the nitroxide. Quantum mechanical calculations indicate that the electron density of the unpaired electron is partitioned almost equally between the oxygen and nitrogen atoms of the nitroxide radical[36] (also observed in our own *ab initio* calculations). The exact population on each atom is known to show dependence on the polarity of the solvent and on fluctuations in the nitroxide structure (*e.g.*, the N–O bond length and the C–N–C angle).[36] For simplicity, we assume that 50% of the electon density is located at the oxygen and the other 50% at the nitrogen sites. Therefore, when calculating the correlation function in eqn (11) from the MD trajectories we used

$$F^{(m)}(\boldsymbol{r}) = [F^{(m)}(\boldsymbol{r}_{\mathrm{Op}}) + F^{(m)}(\boldsymbol{r}_{\mathrm{Np}})]/2, \qquad (25)$$

where $\boldsymbol{r}_{\mathrm{Op}}$ and $\boldsymbol{r}_{\mathrm{Np}}$ correspond to the oxygen–proton and nitrogen–proton distance vectors.

Applying the same logic to the TEMPO–water dimers for which the *ab initio* calculations were performed, we calculated the dipolar coupling tensors given in the last column of Table 3. The agreement with the quantum mechanical calculations is observed to be rather good for conformations 0, 1, and 3. The *ab initio* values are larger for conformations 2 and 4, which also show large scalar coupling. The reason is again the proximity of the water protons to the molecular orbital occupied by the unpaired electron. This geometric proximity is not taken into account when the electron is assumed to be localized at the centers of the oxygen and nitrogen atoms. As in the case of the scalar coupling, we did not attempt to capture this dependence on the dimer geometry when analyzing the MD simulation trajectories. However, we would like to draw attention to the fact that the magnitude of the dipolar coupling in our subsequent analysis is expected to be underestimated exactly for the conformations for which the scalar coupling is largest.

Although the three dipolar correlation functions $C^{(m)}$ are expected to be equal as a result of the orientational isotropy at hand, we extracted all three $F^{(m)}$s from the MD trajectories and calculated the corresponding correlation functions. The correlation functions for $m = 0,1,2$ were observed to be identical within the statistical uncertainty, indicating that the tumbling of TEMPOL with respect to the fixed axes of the simulation box was sampled sufficiently well. The average of the three separate correlation functions was used to calculate the coupling factors. Similarly, to assess the quality of the sampling, the imaginary parts of the correlation functions for $m = 1,2$ were calculated. As expected, they were order(s) of magnitude smaller than the real parts in the time range of up to about 200 ps, which was used for the analysis.

Table 3 Electron-nucleus scalar and dipolar interaction energies (MHz) for the water configurations shown in Fig. 3

Water #	*Ab initio*			Point dipole[a]
	Scalar		Dipolar[b,e]	Dipolar[b]
	bs1[c]	bs2[d]		
0	0.66	0.52	−5.7,−4.4,10.1	−5.6,−5.6,11.2
1	−0.23	−0.31	−6.6,−5.8,12.4	−6.4,−6.2,12.6
2	−3.38	−2.88	−9.2,−8.4,17.6	−6.4,−5.8,12.2
3	0.24	0.11	−6.2,−5.3,11.5	−6.3,−6.0,12.3
4	−3.46	−3.06	−9.1,−8.7,17.8	−6.4,−6.0,12.4

[a] Assuming the unpaired electron is 50% on the oxygen and 50% on the nitrogen atoms. [b] D_{xx},D_{yy},D_{zz} values in principle axis system. [c] Using B3LYP/6-311++G** level of theory. [d] Using B3LYP/aug-cc-pvdz level of theory. [e] Identical values were obtained with both basis sets.

IV. Results

A Correlation functions from MD

Using the MD trajectories at 25, 35 and 45 °C we calculated three different dipolar correlation functions. The normalized correlation functions were fitted to the following functional form

$$a_1 e^{-\tau/\tau_1} + a_2 e^{-\tau/\tau_2} + (1 - a_1 - a_2) e^{-\tau/\tau_3} \qquad (26)$$

in the range of $\tau \in [0,70)$ ps. The resulting fitting parameters are shown in Table 4. From analytical treatments it is known that for long times the dipolar correlation function exhibits a

Table 4 Time scales τ_i (ps) and amplitudes a_i used to fit the the normalized correlation functions at the specified temperature T (°C)

	T		τ_1	τ_2	τ_3	a_1	a_2	a_3[a]	a_{pow}
		O–N	0.38	4.12	29.0	0.273	0.468	0.259	16.56
	25	O	0.25	3.08	23.7	0.299	0.516	0.185	8.75
Dipolar		N	0.87	8.41	39.9	0.232	0.437	0.331	34.3
	35	O–N	0.44	4.44	29.1	0.325	0.476	0.199	12.81
	45	O–N	0.42	4.14	27.0	0.340	0.487	0.173	9.95
Scalar	25	O–N	1.57	13.3	122	0.546	0.428	0.026	—

[a] This coefficient was constrained to $a_3 = 1 - a_1 - a_2$.

power law decay with exponent −1.5. The coefficient in $a_{pow}\tau^{-3/2}$ was chosen such that the curve is tangent to the exponential fit. The calculated correlation functions and the best fits are plotted in Fig. 4. It is seen that the tails of the correlation functions follow closely the power law decays from the point where the exponential fit departs from the data ($\tau \approx 30$ ps) up to $\tau \approx 200$ ps. The departure of the calculated correlation functions from the power law at longer times is a finite-size effect, which becomes more pronounced at the higher temperatures where the water diffusion is faster.

For the purposes of comparison, two additional dipolar correlation functions were calculated from the MD simulations at 25 °C assuming that the unpaired electron is localized entirely at the oxygen or the nitrogen atoms of the radical. The fitting parameters in these cases are denoted, respectively by O and N in Table 4.

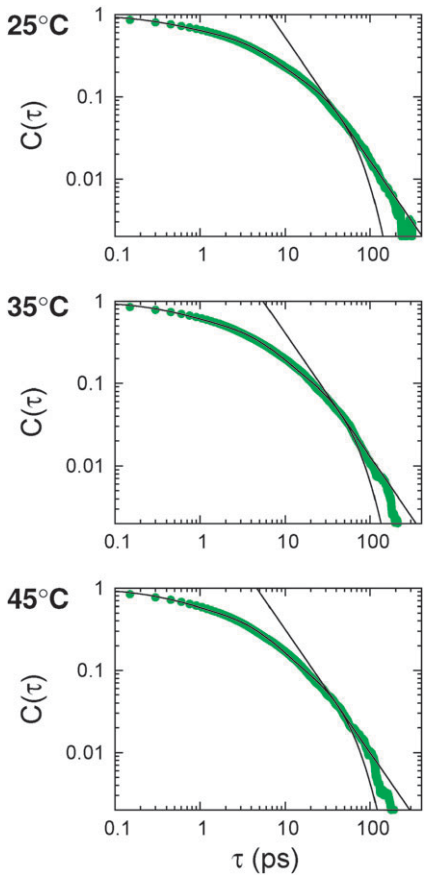

Fig. 4 Normalized dipolar correlation functions at the specified temperature (thick dots) and best fits (thin lines). The straight lines tangent to the correlation functions correspond to the asymptotic power-law decay implied by the analytical FF model (see text).

In principle, one can calculate the dipolar spectral densities from the raw correlation functions performing numerical Fourier transformations. However, we preferred to first fit the correlation functions and subsequently work with the fitting functions for several reasons. The fit to a sum of exponential decays allows us to talk about the various time scales associated with the solute–solvent dynamics. Substantial relative TEMPOL–water motion is seen to occur on well-separated time scales of about 0.4, 4, and 30 ps (Table 4), the last of which connects to the small-amplitude but long-lasting dynamics captured by the $\sim\tau^{-3/2}$ tail of the correlation function. About 30% of the correlation function is seen to decay on a sub-picosecond time scale, whereas almost 50% decays in a few ps. Such fast dynamics is essential for the efficiency of the Overhauser-based nuclear enhancement at high magnetic fields. As mentioned before, the long-time tail of the computed correlation functions is expected to be degraded by finite size effects. Thus, enforcing the $\tau^{-3/2}$ decay analytically should provide a better estimate of the integrated area under the correlation function (*i.e.*, the spectral density at very low frequencies). This is important since the larger the spectral density at the nuclear Larmor frequency the smaller the high-field coupling factor [*cf.* eqn (17)].

Before proceeding with the calculation of the DNP coupling factors we attempted to assess whether the contribution of the spectral density $K(\omega)$ is indeed negligible compared to the contribution of $J(\omega)$. To this end, the correlation function corresponding to the scalar coupling model (14) was calculated using the values $A_0 = 3$ MHz, $r_0 = 1.9$ Å, and $\lambda^{-1} = 0.8$ Å. The normalized correlation function, calculated from the MD trajectories at 25 °C, is shown in Fig. 5 together with the best fit of the form given in eqn (26). The fitting was performed for $\tau \in [0,400)$ ps and yielded the fitting parameters listed in the last row of Table 4.

Table 5 shows the values of the spectral densities $J_{norm}(\omega)$ and $K_{norm}(\omega)$ calculated from the corresponding normalized correlation functions at 25 °C. The magnitudes are seen to be comparable over the whole frequency range. Accounting for the differences due to the normalization of the correlation functions and for the division of $K(\omega)$ by δ^2 in eqn (16), it becomes apparent that the contribution of the scalar coupling amounts to less than 2% of the contribution of the dipolar coupling to the numerator of eqn (16). The actual contribution

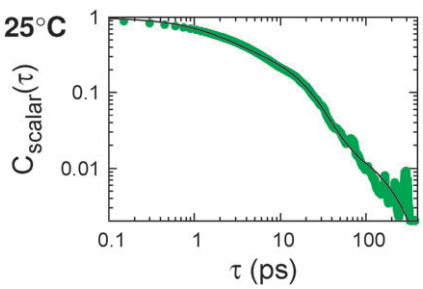

Fig. 5 Normalized scalar correlation functions at 25 °C (thick dots) and best fit (thin line).

Table 5 Spectral densities at $\omega = 2\pi f$ calculated from the fits to the normalized dipolar and scalar correlation functions at 25 °C

f/GHz	0	9.6	34	94	180	260	360
J_{norm}[a]	12.9	3.85	1.38	0.403	0.179	0.120	0.083
K_{norm}[b]	9.72	4.37	1.40	0.552	0.232	0.125	0.069

[a] To be multiplied by 4.31×10^{-1} to recover J before normalization. [b] To be multiplied by $35.2/\delta^2 = 5.65 \times 10^{-3}$ for direct comparison with the contribution of the dipolar coupling.

is expected to be somewhat smaller given our choice of $A_0 = 3$ MHz for all hydrogen bonding geometries. Thus, we conclude that the influence of the scalar coupling on the DNP coupling factors is negligible over the whole frequency range. In the following we use the approximate expression (17) to calculate the coupling factor.

B Coupling factors from MD

The DNP coupling factors at magnetic field strengths ranging from 0.33 to 12 Tesla were calculated using eqn (17) and the fitting parameters given in Table 4. The results are shown in Table 6. As expected, the coupling factors decrease substantially upon increase in the magnetic field. The coupling factors calculated here from first principles are in good agreement with the values determined from NMRD measurements at 9.6, 94,[5] and 260 GHz.[8] Our calculated value of 30% at 9.6 GHz is somewhat lower than the experimental (NMRD) value of 36%,[5] but substantially higher than the value of 18%, which was deduced form DNP enhancement measurements at 9.8 GHz for an aqueous solution of a nitroxide (4-oxo-TEMPO) very similar to TEMPOL.[14] Recently, the latter coupling factor has been corrected to 22%,[15] which is somewhat closer to the NMRD value with the MD value falling in between. (The MD value for 9.8 GHz is 29.6%.) We will have more to say about the NMRD estimates of the coupling factors in section IVD.

As expected, the values in Table 6 indicate more efficient coupling with increasing temperature. Also, the calculated DNP enhancements at a given field and temperature show high sensitivity to the distance of closest approach between the electronic and nuclear spins. At 260 GHz, for example, roughly four times larger enhancement is calculated for the oxygen-based electron (2.94%) compared to the nitrogen-based one (0.79%). The comparison of these two extreme cases is intended to illustrate the dramatic effect of moving the electron spin from the surface toward the interior of the radical. The rapid ($1/r^6$) decrease of the dipolar interaction with distance, which is responsible for the effect, provides a rational for the poor coupling factor of the bulkier TAM (trityl) radical deduced to be only 1.8% at 40 GHz.[4]

Table 6 Coupling factors ($\times 10^{-2}$) at the given frequencies (in GHz) calculated from the fits to the MD correlation functions

T/°C		9.6[a]	34	94[b]	180	260[c]	360
	O–N	**29.9**	**15.0**	**5.34**	**2.58**	**1.80**	**1.30**
25	O	34.2	20.9	9.18	4.33	2.94	2.17
	N	25.0	8.50	2.57	1.26	0.79	0.49
35	O–N	32.0	17.5	6.60	3.42	2.43	1.74
45	O–N	33.9	20.0	8.00	4.17	2.97	2.15

[a] The experimental (NMRD) value at this frequency is 36 ± 2.[5] [b] The experimental (NMRD) value is 6 ± 2.[5] [c] The experimental value is 2.2 ± 0.6.[8]

C Comparison with the force-free model

The analytical FF model contains two physical parameters, the diffusion coefficient D_{ff} and the distance of closest approach d_{ff}. The connection to the coupling factors is through the time scale τ_{ff}, given in eqn (21). One can, therefore, compare the MD results with the analytical model along two lines. The first approach would be to calculate τ_{ff} from D_{ff} and d_{ff}, where the latter are extracted directly from the MD simulations. The coefficient of relative translational diffusion is the sum of the translational diffusion coefficients of water and TEMPOL, $D_{ff} = D_{Tw} = D_w + D_T$. For the distance of closest approach between the proton spin and the electron spin we can calculate two values, d_{Op} and d_{Np}, assuming the electron is localized at the oxygen or the nitrogen, respectively. An alternative way of comparison would be to calculate τ_{ff} from the coupling factors in Table 6 using eqn (22) and (17).

At this point, it is necessary to stress that the FF treatment assumes spherical spin-bearing molecules which can approach each other down to a distance d_{ff} from every direction. Clearly, these assumptions do not hold for TEMPOL and water. The distance of closest approach in the analytical treatment, therefore, should be viewed as an effective distance which does not necessarily correspond to d_{Op} or d_{Np}. Nevertheless, even if only to illustrate this point more convincingly, we believe it is worthwhile to carry out the proposed comparison.

Bearing this in mind, we calculated the translational diffusion coefficient of TEMPOL in water, D_T, and determined the distances of closest approach using the MD trajectories at 25 °C. The results are shown in Table 7. Very encouraging is that the MD estimate of the translational diffusion coefficient D_T is in perfect agreement with the experimental value of 0.41×10^{-9} m^2 s^{-1} reported recently for TEMPONE.[15] The time scales τ_{ff} deduced from D_{Tw} and d_{Op} or d_{Np} are also shown in Table 7. Not surprisingly, the shorter distance d_{Op} leads to a shorter time scale compared to d_{Np}. For an electron which is delocalized on the oxygen and nitrogen atoms the time scale is expected to lie between the calculated values of τ_{Op} and τ_{Np}, and therefore be bounded from above by ≈ 16 ps.

As mentioned before, the time scales τ_{ff} can be calculated using the coupling factors from the MD simulations and the analytical spectral density. The results are shown in Table 8 for the simulation carried out at 25 °C and the coupling factors highlighted in bold in Table 6. From these time scales, and using the relative diffusion coefficient D_{Tw} estimated from the MD simulations, it is possible to calculate effective distances of

Table 7 Translational diffusion coefficients D (10^{-9} m^2 s^{-1}), the distances of closest approach d (Å) and the calculated time scales, $\tau = d^2/D_{Tw}$ (ps), for the TEMPOL oxygen (O) or nitrogen (N) and water proton (p)

D_w	D_T	D_{Tw}	d_{Op}	d_{Np}	τ_{Op}	τ_{Np}
2.3[a]	0.4	2.7	1.59	2.06	9.4	16

[a] Experimental value from ref. 29.

Table 8 Time scales τ_{ff} (ps), calculated from the coupling factors in Table 4; "distances of closest aproach" d_{ff} (Å) calculated from τ_{ff}

GHz	9.6	34	94	180	260	360
τ_{ff}	43.9	35.2	30.5	25.9	22.5	19.8
d_{ff}[a]	3.44	3.08	2.87	2.64	2.46	2.31

[a] Calculated as $d_{ff} = (\tau_{ff} D_{Tw})^{1/2}$ for $D_{Tw} = 2.7 \times 10^{-9}$ m^2 s^{-1}.

closest approach, d_{ff}. Those are shown in the last row of Table 8.

It is not surprising that all of the τ_{ff}s in Table 8 are actually larger than the 16 ps upper bound which was estimated above using the distance d_{Np}. As already discussed, in the MD simulations (and presumably in reality) the distances of closest approach d_{Op} and d_{Np} are not attainable from every direction, contrary to the assumptions of the analytical treatment. What is more interesting is that the time scales τ_{ff} calculated directly from the MD coupling factors have a strong frequency dependence. In the range of frequencies studied here, τ_{ff} changes by a factor of two. Similarly, the distances of closest approach inferred from the calculated values of τ_{ff} are seen to decrease with increasing field strength. On a very descriptive level this trend can be interpreted as an indication that the DNP coupling factors at higher fields probe shorter molecular distances and faster molecular dynamics.

D On the NMRD estimates of the coupling factor

The discrepancy between the coupling factors estimated from NMRD measurements at 9.6 GHz,[5] DNP enhancement data at 9.8 GHz[15] and our MD simulations is noteworthy considering the claim in ref. 15 that the NMRD estimate at this frequency is likely flawed and the coupling factor of 22%, deduced from DNP enhancement measurements, should be considered as more reliable. Hoping to explore at least some of the possible sources of ambiguity in calculating coupling factors from NMRD data using the approximate eqn (19), here we look at the NMRD estimation procedure of ref. 5 and 8 from the perspective of the MD simulations. To this end, we examine how the coupling factors are affected by the assumption X = const. in eqn (20). The "experimental" information in our case are the spectral densities that appear in eqn (20). These are calculated from the MD simulations.

First, we ask the following question: what are the values of X that need to be used in eqn (20) in order to obtain exactly the MD coupling factors for 25 °C (given in Table 6)? Of course, the correct answer is to use $X = 3J(\omega_I)$. These values (up to an arbitrary but constant normalization factor) are given in the first row of Table 9 for the three frequencies studied experimentally. It is immediately seen that the correct values of X do depend on the frequency of interest, contrary to the assumption behind eqn (20) [or its equivalent eqn (19)].

Next, to assess how important this variation in X over the frequency range is, we calculate the coupling factors at 9.6, 94 and 260 GHz using eqn (20) and keeping X constant at the three X_{MD} values in Table 9. The results are given in the first three columns of Table 10. As expected, the original MD values are recovered along the diagonal. The dashes in the last row indicate that the estimated coupling factors are

Table 9 Values of $X = 3J(\omega_I)$ at the given frequencies (f_S) calculated from the spectral densities deduced from the MD simulations and the FF model

X	9.6 GHz	94 GHz	260 GHz
$X_{MD}(\omega_I)$	37.47	34.94	32.47
$X_{ff}(\omega_I)$	37.96[a]	35.16[a]	32.47[a]

[a] X_{ff}s are normalized by a common scaling factor such that the value at 260 GHz is the same as the MD value.

meaningless since the value of X is larger than $3J(\omega_I) + 7J(\omega_S)$ at this frequency. We notice that with the choice $X = 32.47$, which recovers our calculated coupling factor at 260 GHz, the estimate at 9.6 GHz is 35.4%. This value is in perfect agreement with the experimental estimate of 36%. However, the corresponding coupling of 10% at 94 GHz is substantially larger than the experimental estimate of 6%. In the last two columns of Table 10 we present the coupling factors calculated using eqn (20) with different choices of the constant X. The bold numbers are within the error bars of the experimental estimates. It is apparent that it is not possible to simultaneously rationalize all the three NMRD values in terms of the spectral densities obtained from the MD simulations and the assumption of constant X in eqn (20).

Finally, it should be mentioned that the variation of X, or $J(\omega_I)$, in the examined frequency range should be rather insensitive to the details of the molecular motion captured by the MD simulations. Instead, the long-time tail of the dipolar correlation function and its total integrated area are expected to be most important. Given that we imposed the long-time behavior of the FF model as the asymptote of the MD correlation function, one would expect that the analysis of this section could have been performed using the spectral density of the FF model, eqn (22). That this is indeed the case is demonstrated in the last row of Table 9, which shows that the frequency dependence of X according to this model is essentially identical to the frequency dependence resulting from the MD simulations.

E Water–nitroxide hydrogen bonding dynamics

As already stated before, in principle it is not necessary to fit the MD correlations functions to any functional form, including the one given in eqn (26), in order to take their Fourier transform and calculate the corresponding spectral densities. In that sense, the choice of the multiexponential decay is arbitrary and is not motivated by a dynamical model. The only justification for this choice is that it fits the data well in the range of up to 30–40 ps, after which the $\sim\tau^{-1.5}$ asymptote appears to take over. Nevertheless, the different time scales identified with the multiexponential fit raise the question of what physical processes might be causing them. In

Table 10 Coupling factors ($\times 10^{-2}$) calculated using eqn (20) and the given values of X

X	37.47	34.94	32.47	33.6	32.3
9.6 GHz	29.9	32.7	35.4	**34.2**	**35.6**
94 GHz	0.54	5.33	10.0	**7.87**	10.3
260 GHz	—	—	1.80	—	**2.16**

an effort to shed light on this question, we analyzed the hydrogen bonding events between TEMPOL and water contained in the MD trajectories.

Typically, a given geometry is classified as a hydrogen bonding event on the basis of the distance between the hydrogen bonded species and the hydrogen-bond angle (*i.e.*, the distance between the heavy atoms O and X and the angle O–H···X). In our analysis the cutoffs for the hydrogen bond distance and angle were 4.5 Å and 150°. In other words, a water molecule whose oxygen atom was within 4.5 Å of the nitroxide oxygen (X) and for which the O–H···X angle was larger than 150° was considered to be hydrogen bonded to the radical. Once identified, the hydrogen bonding events were grouped according to their lifetime.

A histogram of the hydrogen bonding events *versus* their life times (bin width of 2 ps) is shown in Fig. 6. The majority of the events nicely follow an exponential decay with a time constant of 3.6 ps (the straight line in the Figure). The only exceptions are at the two extremes of very short- and very long-lived hydrogen bonds. The events in the first bin, with life times less than 2 ps, correspond to waters which transiently approach the nitroxide within less than 4.5 Å and quickly diffuse away. During the 2 ns simulation time, four events were observed to have rather long life times, between 30 and 32 ps (last bin).

From the data in Fig. 6 we conclude that the mean lifetime of the hydrogen bonded water–nitroxide complex is 3.6 ps, according to the MD simulations. This number is very similar to the intermediate time scale of ≈4.1 ps emerging from the multiexponential fits to the dipolar correlation functions. For the purposes of visualizing the various "modes of motion" that lead to the identified time scales, we thus speculate that the fast thermal librations of the water molecules that are hydrogen bonded to the nitroxide moiety lead to the fast decay (≈0.4 ps), the forming and breaking of these hydrogen bonds is responsible for the intermediate decay (≈4 ps), and the large-scale translational diffusion of the waters accounts for the long decay (≈30 ps) and the asymptote of the dipolar correlation function. Only this last process of relative translational diffusion is expected to be properly described by the FF model.

In addition to the proposed processes, other molecular motions should also contribute to both of the faster time scales. For example, depending on the nitroxide–water hydrogen bonding geometry, the dynamics of the second hydrogen, which is not engaged by the nitroxide moiety, could also modulate the dipolar interaction appreciably. The hydrogen bond dynamics between two water molecules adjacent to the nitroxide surface is therefore expected to affect the initial decay of the dipolar correlation function. The ability of MD simulations to follow all these simultaneous processes, which likely span a range of overlapping time scales, makes them perfectly suited for the calculation of DNP coupling factors between small molecules.

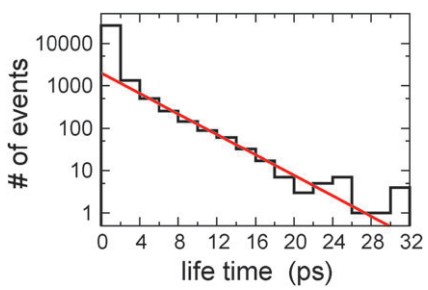

Fig. 6 Histogram of the hydrogen bonding events *versus* their life times (in steps of 2 ps). The straight line is an exponential decay with a time constant of 3.6 ps.

Admittedly, the proposed correspondence between these intuitive motions and the time scales identified by the multiexponential fit to the dipolar correlation functions is an oversimplification. This is exemplified by the fits at 25 °C in Table 4. Whereas the time scales associated with concrete physical processes are not expected to change depending on the assumed location of the unpaired electron, the decays of the correlation functions for oxygen- and nitrogen-based electron spin differ substantially. The dipolar interaction used to report on the microscopic dynamics filters this information in a complex distance- and angle-dependent way. The outcome, therefore, is sensitive to the underlying molecular geometry in ways which may not be directly relevant for the basic "modes of motion." This poses a substantial difficulty in reading out the fundamental motional time scales from the decay of the dipolar correlation function.

V. Discussion

Dynamic nuclear polarization coupling factors were computed using dipolar time correlation functions obtained directly from molecular dynamics simulations of the nitroxide radical TEMPOL in water at three different temperatures. The calculated correlation functions contain information about the relative motions of the water protons and the nitroxide over a broad range of time scales, starting from a fraction of a picosecond. A single correlation function was used to calculate DNP coupling factors as a function of the magnetic field strength for the range from 0.34 to 12.8 Tesla.

The calculated coupling factors are in good agreement with the available experimental values for TEMPOL in water at 0.34, 3.4,[5] and 9.2 Tesla,[8] deduced from NMRD measurements. As a cross check, the assumption of constant $2\omega_1$ in eqn (19), which was used to obtain the experimental coupling factors, was scrutinized on the basis of the MD simulations. This analysis indicated that the assumption is not entirely justified and likely causes additional uncertainties in the NMRD estimates of the coupling factors on top of the reported error bars. Nevertheless, the MD simulations and the NMRD data are in overall agreement. This implies that the relative nitroxide–solvent dynamics in a time range from 0.4 to 17 ps (reflected by the magnitude of the spectral density function at the Larmor frequency of the electron) and further up to hundreds of picoseconds (reflected by the spectral density at the nuclear Larmor frequency) was captured rather well by the MD simulations. Important in this respect was the calibration of the water diffusion coefficient, which enforced the correct long-time behaviour.

Only dipolar coupling between the electron and nuclear spins was considered in the calculation of the coupling factors. Combining *ab initio* calculations with the MD simulations we

have presented evidence that it is indeed legitimate to ignore the scalar coupling of the spins.

Reinterpreting the coupling factors calculated from the MD simulations in the context of the FF model of translational diffusion, we drew attention to the fact that it is not possible to use this model to reliably describe the field dependence of the DNP data. The analytical model is very useful when the goal is to assess the effect of temperature on the DNP coupling factor (by appropriately scaling the relative diffusion coefficient D_{ff}) or the influence of the accessibility of the electron spin to water (by changing the distance of closest approach d_{ff}). In such cases, the parameters of the model provide valuable intuitive understanding appropriate for order-of-magnitude analysis of the trends. However, direct identification of the parameters of the analytical approach with molecular properties (*i.e.*, atomistic distance of closest approach and known diffusion coefficients) is actually problematic. From that perspective, the analytical parameters should be viewed as "effective" distance of closest approach or "effective" relative diffusion, the values of which can vary with frequency. In the same vein, we think that the interpretation of NMRD data through fits to increasingly more complex motional models can greatly benefit from the use of MD simulations to restrict the values of some of the fitting parameters.

Attempts to go beyond the FF model of translational diffusion by imposing known radial distribution functions[16] or allowing for off-centered spins[37] exist but are harder to use for fitting to experimental data since they do not necessarily lead to closed-form analytic expressions. The philosophy of the current paper is fundamentally different. Rather than trying to develop a more realistic, analytically or numerically tractable fitting model we deduce the relevant dynamical time scales from all-atom MD simulations. This atomistic description automatically takes into account the various types of solute–solvent motions which have been considered in the literature such as the relative translational diffusion of the two spin species, the rotational diffusion of the off-centered spins, and the rotational diffusion of the supposedly tightly bound water–nitroxide complex. In addition, these diffusive motions naturally experience the potential of mean force due to the molecular pair-correlation functions.

However, it is important to realize that the classical MD approach might become increasingly inappropriate at even shorter time scales. For example, the classical energy function (force field) that was used does not explicitly account for the lone electron pairs on the oxygen atoms of the nitroxide or water. Therefore, the coordination of the nitroxide oxygen by the nearest water molecules is not expected to be exactly correct. (For a systematic comparison of the nitroxide–water interaction geometries and energies with quantum mechanical calculations see ref. 30.) In addition, both the water and the nitroxide models used in this study lack an explicit description of the atomic polarization. The polarizability (or its absence thereof) is known to be largely responsible for the fast diffusion of the TIP3P and other nonpolarizable water models. We have partially addressed this issue by artificially slowing down the water dynamics. Nevertheless, it is not clear to what extent the increased friction that we introduced and the lack of polarizability affect the fast sub-picosecond dynamics. Furthermore, on increasingly shorter time scales it might be necessary to explicitly account for at least some quantum mechanical effects. For example, the population of the unpaired electron is known to redistribute between the nitrogen and oxygen atoms of the nitroxide upon hydrogen bonding. Again, such effects were neglected in the present study, where the electron was assumed to be localized at the centers of these atoms in a 1 : 1 ratio.

Given all these approximations inherent in the MD simulations, we have not sought means to improve on the description of the scalar and dipolar interactions beyond the functional form (14) and the point dipole approximation. Admittedly, these approximations fail for some of the water molecules in direct contact with the nitrogen or oxygen atoms of the nitroxide, as is clearly demonstrated in Table 3. Certainly, using more sophisticated and realistic forms for the scalar coupling is conceivable. However, even if we imagine that the calculated contribution of the scalar coupling increases by a factor of two as a result of that (which is rather unlikely), its relative importance with respect to the dipolar contribution will remain less than 5%. On the other hand, since the point dipole approximation can only become better with increasing distance, the dipolar interaction is *underestimated* by about 30% for at most two water molecules out of all the simulated waters. Thus, neither of these approximations is expected to change the conclusion that the calculated DNP coupling factors at the higher magnetic fields are substantially larger than what is expected from extrapolations based on the FF model.

Unlike the value of the DNP enhancement, the value of the coupling factor is not directly accessible experimentally. Recently there has been a systematic effort to quantify the degree of electron spin saturation and thus access the coupling factor from DNP enhancement measurements [*cf.* eqn (9)].[14] It has been claimed that this approach yields more reliable coupling factors compared to the estimates based on NMRD measurements.[15] In ref. 15, the coupling factor of TEMPONE in water at 9.8 GHz was estimated to be 22%. (The MD value for TEMPOL at this frequency is 29.6%.) Somewhat disconcerting however is that this value had been reported as 18% in a previous work by the same authors.[14] The difference was explained to be due to the more powerful microwave source employed in the later study.[15] However, the available microwave power should affect only the degree of saturation and not the coupling factor. Clearly, for the reliable determination of the coupling factor from DNP enhancement data, the estimated saturation should reflect the experimental conditions (including the given microwave power).

The measured DNP enhancements at 3.4[5] and 9.2 Tesla[8] provide support for the coupling factors at these higher fields computed in the present article. Nevertheless, direct quantitative comparison with the experimental DNP enhancements is hindered by the uncertainties associated with the saturation factor. A rigorous theoretical analysis of the saturation under the experimental conditions and a direct comparison with experiments at 9.2 T is carried out in the companion paper.

VI. Conclusion

The results of this study demonstrate that DNP coupling factors over a wide range of field strengths of experimental interest can be calculated reliably using all-atom molecular

dynamics simulations. This opens the possibility to move beyond the understanding offered by analytical motional models, which assume spherical spin-bearing molecules. Therefore, one can start addressing the molecular detail of the solvent or the polarizing agent and study their influence on the coupling factor. Such knowledge is expected to be useful in designing and synthesizing polarizing agents properly "tuned" to the desired solvent such that maximal DNP enhancement is achieved.

However, when employing MD simulations to calculate the coupling factor, care has to be taken of the unrealistically large water diffusion coefficient, a feature common to all the non-polarizable water models.[28] Undoubtedly, the most natural way to avoid this problem is to employ a polarizable force field. Such force fields exist for water and are currently under active development and improvement for larger biomolecules like proteins and DNA. Nevertheless, our results indicate that a nonpolarizable water model can be successfully employed if its diffusion is calibrated to match the experimental value by adjusting the friction of the Langevin thermostat. Therefore, it should be possible to adopt the approach presented here to study computationally the DNP of water or other solvents by different mono- or bi-radicals using the existing non-polarizable force fields. Our own studies of nitroxide biradicals in water using the methodology of this paper will be reported elsewhere.

Acknowledgements

D. S. is indebted to Prof. Benoît Roux for suggesting the method employed in the present study to correct the diffusion of the water model, and to Dr Bela Bode for stimulating discussions about the *ab initio* calculation of the scalar couplings. We thank the two anonymous reviewers for their constructive feedback. This work was funded by the European Union BioDNP Project.

References

1 K. H. Hausser and D. Stehlik, *Adv. Magn. Reson.*, 1968, **3**, 79.
2 W. Müller-Warmuth and K. Meise-Gresch, *Adv. Magn. Reson.*, 1983, **11**, 1.
3 R. D. Bates and W. S. Drozdoski, *J. Chem. Phys.*, 1977, **67**, 4038.
4 R. Wind and J.-H. Ardenkjaer-Larsen, *J. Magn. Reson.*, 1999, **141**, 347.
5 P. Höfer, G. Parigi, C. Luchinat, P. Carl, G. Guthausen, M. Reese, T. Carlomagno, C. Griesinger and M. Bennati, *J. Am. Chem. Soc.*, 2008, **130**, 3254.
6 M. Prandolini, V. P. Denysenkov, M. Gafurov, S. Lyubenova, B. Endeward, M. Bennati and T. Prisner, *Appl. Magn. Reson.*, 2008, **34**, 399.
7 V. P. Denysenkov, M. J. Prandolini, A. Krahn, M. Gafurov, B. Endeward and T. F. Prisner, *Appl. Magn. Reson.*, 2008, **34**, 289.
8 M. J. Prandolini, V. P. Denysenkov, M. Gafurov, B. Endeward and T. F. Prisner, *J. Am. Chem. Soc.*, 2009, **131**, 6090.
9 P.-O. Westlund and R. M. Lynden-Bell, *J. Magn. Reson.*, 1987, **72**, 522.
10 M. Luhmer, A. Moschos and J. Reisse, *J. Magn. Reson., Ser. A*, 1995, **113**, 164.
11 J.-P. Grivet, *J. Chem. Phys.*, 2005, **123**, 034503.
12 A. Abragam, *The Principles of Nuclear Magnetism*, Oxford University Press, New York, 1961.
13 J. B. Pedersen and J. H. Freed, *J. Chem. Phys.*, 1973, **58**, 2746.
14 B. D. Armstrong and S. Han, *J. Chem. Phys.*, 2007, **127**, 104508.
15 B. D. Armstrong and S. Han, *J. Am. Chem. Soc.*, 2009, **131**, 4641.
16 L.-P. Hwang and J. H. Freed, *J. Chem. Phys.*, 1975, **63**, 4017.
17 Y. Ayant, E. Belorizky, J. Alizon and J. Gallice, *J. Phys.*, 1975, **36**, 991.
18 J. H. Freed, *J. Chem. Phys.*, 1978, **68**, 4034.
19 C. F. Polnaszek and R. G. Bryant, *J. Chem. Phys.*, 1984, **81**, 4038.
20 I. Bertini, C. Luchinat and G. Parigi, *Solution NMR of Paramagnetic Molecules*, Elsevier, 2001.
21 J. Kowalewski and L. Mäler, *Nuclear Spin Relaxation in Liquids: Theory, Experiments and Applications*, Taylor and Francis, 2006.
22 W. L. Jorgensen, J. Chandrasekhar, J. D. Madura, R. W. Impey and M. L. Klein, *J. Chem. Phys.*, 1983, **79**, 926.
23 J. C. Phillips, R. Braun, W. Wang, J. Gumbart, E. Tajkorshid, E. Villa, C. Chipot, R. D. Skeel, L. Kale and K. Schulten, *J. Comput. Chem.*, 2005, **26**, 1781.
24 T. Darden, D. York and L. Pedersen, *J. Chem. Phys.*, 1993, **98**, 10089.
25 U. Essmann, L. Perera, M. L. Berkowitz, T. Darden, H. Lee and L. G. Pedersen, *J. Chem. Phys.*, 1995, **103**, 8577.
26 S. Miyamoto and P. A. Kollman, *J. Comput. Chem.*, 1992, **13**, 952.
27 G. Lamoureux, A. D. MacKerell and B. Roux, *J. Chem. Phys.*, 2003, **119**, 5185.
28 P. Mark and L. Nilsson, *J. Phys. Chem. A*, 2001, **105**, 9954.
29 R. Mills, *J. Phys. Chem.*, 1973, **77**, 685.
30 D. Sezer, J. H. Freed and B. Roux, *J. Phys. Chem. B*, 2008, **112**, 5755.
31 A. D. MacKerell, Jr, D. Bashford, M. Bellott, R. Dunbrack, Jr, J. Evanseck, M. Field, S. Fischer, J. Gao, H. Guo and S. Ha, *et al.*, *J. Phys. Chem. B*, 1998, **102**, 3586.
32 M. Schlenkrich, J. Brickmann, A. MacKerell, Jr and M. Karplus, in *Biological Membranes: A Molecular Perspective from Computation and Experiment*, Birkhauser, Boston, 1996, pp. 31–81.
33 M. J. Frisch, G. W. Trucks, H. B. Schlegel, G. E. Scuseria, M. A. Robb, J. R. Cheeseman, J. A. Montgomery, Jr., T. Vreven, K. N. Kudin, J. C. Burant, J. M. Millam, S. S. Iyengar, J. Tomasi, V. Barone, B. Mennucci, M. Cossi, G. Scalmani, N. Rega, G. A. Petersson, H. Nakatsuji, M. Hada, M. Ehara, K. Toyota, R. Fukuda, J. Hasegawa, M. Ishida, T. Nakajima, Y. Honda, O. Kitao, H. Nakai, M. Klene, X. Li, J. E. Knox, H. P. Hratchian, J. B. Cross, V. Bakken, C. Adamo, J. Jaramillo, R. Gomperts, R. E. Stratmann, O. Yazyev, A. J. Austin, R. Cammi, C. Pomelli, J. Ochterski, P. Y. Ayala, K. Morokuma, G. A. Voth, P. Salvador, J. J. Dannenberg, V. G. Zakrzewski, S. Dapprich, A. D. Daniels, M. C. Strain, O. Farkas, D. K. Malick, A. D. Rabuck, K. Raghavachari, J. B. Foresman, J. V. Ortiz, Q. Cui, A. G. Baboul, S. Clifford, J. Cioslowski, B. B. Stefanov, G. Liu, A. Liashenko, P. Piskorz, I. Komaromi, R. L. Martin, D. J. Fox, T. Keith, M. A. Al-Laham, C. Y. Peng, A. Nanayakkara, M. Challacombe, P. M. W. Gill, B. G. Johnson, W. Chen, M. W. Wong, C. Gonzalez and J. A. Pople, *GAUSSIAN 03 (Revision C.02)*, Gaussian, Inc., Wallingford, CT, 2004.
34 W. S. Benedict, N. Gailar and E. K. Plyler, *J. Chem. Phys.*, 1956, **24**, 1139.
35 P. R. Rablen, J. W. Lockman and W. L. Jorgensen, *J. Phys. Chem. A*, 1998, **102**, 3782.
36 M. Pavone, P. Cimino, O. Crescenzi, A. Sillanpaa and V. Barone, *J. Phys. Chem. B*, 2007, **111**, 8928.
37 B. Halle, *J. Chem. Phys.*, 2003, **119**, 12372.